



Cite this: *Phys. Chem. Chem. Phys.*,  
2016, **18**, 30931

## Polyelectrolytes adsorbed at water–water interfaces

R. Hans Tromp,<sup>ab</sup> Remco Tuinier<sup>bc</sup> and Mark Vis<sup>\*c</sup>

Polyelectrolytes can show strong adsorption at water–water interfaces formed by phase separation of two polymers in aqueous solution. We demonstrate this for a model system consisting of neutral polymer A and weakly positively charged polymer B. When polyelectrolyte is added with similar chemical composition as polymer A, but charge of opposite sign as polymer B, interfacial accumulation is observed. We hypothesize this accumulation to be complexation at the water–water interface. This adsorption surprisingly persists even at high salt concentrations and has only a limited effect on the interfacial tension. Complexation of polyelectrolytes at water–water interfaces may provide a new path towards the stabilization of water-in-water emulsions.

Received 4th October 2016,  
Accepted 31st October 2016

DOI: 10.1039/c6cp06789a

www.rsc.org/pccp

### 1 Introduction

Complex coacervation has been a widely studied subject for many years<sup>1–7</sup> and is, at least qualitatively, well understood. It is the complexation of positively and negatively charged polymers, usually in water, and the subsequent macroscopic equilibrium phase separation, where one phase is enriched in both polymers and the other is depleted of both polymers. Complex coacervation is understood to be mainly driven by an increase in entropy of counterions upon complexation: after complexation, the charged polymers neutralise each other and the counterions are liberated into solution. An enthalpic effect of the association of the oppositely charged polymers may also play a (secondary) role.

In contrast to the associative phase separation that occurs during complex coacervation, segregative phase separation between two polymer-enriched phases is also known to occur in (aqueous) solutions of two polymers.<sup>8,9</sup> In this case, the polymers should be uncharged, weakly charged or like-charged.<sup>10</sup> The phase separation is driven by the non-favourable enthalpy of mixing the two polymers, resulting in two phases each enriched in one of the polymers. Both phases contain a similar high concentration of water, often over 90%. Therefore, the interface separating the two coexisting aqueous phases is commonly called a water–water interface and such systems may be denoted aqueous two-phase systems.

Water–water interfaces have intriguing properties: they have an ultralow interfacial tension,<sup>11–14</sup> they are fully permeable to solvent and small solutes;<sup>15</sup> when compared to coexisting polymer blends or oil–water interfaces, they have a relatively large thickness;<sup>16,17</sup> and, if one of the polymers is weakly charged, the interface is also charged.<sup>18</sup> This interfacial charge further reduces the interfacial tension.<sup>19</sup>

In this paper we focus on another property of water–water interfaces, namely the possibility of complexation of polyelectrolytes at water–water interfaces.

Two recent examples of interfacial complexation were presented by Ma *et al.*<sup>20</sup> and Hann *et al.*<sup>21</sup> who used neutral phase separating polymers in aqueous solution. To their systems, two oppositely charged polyelectrolytes were added, one in each phase. When the polyelectrolytes diffused towards the other phase and towards each other, they formed a complex at the water–water interface, which stabilized emulsion droplets.

Our present work originates from work on water-in-water Pickering emulsions formed by aqueous mixtures of dextran and gelatin. The intention was to stain the dextran-rich emulsion droplets with a small amount of fluorescently labelled dextran (FITC-dextran) for observation by confocal microscopy.<sup>17</sup> However, it turned out that the fluorescent dextran did not at all stain the dextran-rich phase. Instead, it accumulated primarily at the water–water interface and to lesser extent in the gelatin-rich phase: confocal microscopy showed water-in-water emulsion droplets encircled by bright rings, as can be seen in Fig. 1. These observations inspired us to perform self-consistent field (SCF) computations on an idealized model system to investigate another route towards complexation at water–water interfaces.

We propose to achieve interfacial complexation by using an aqueous mixture of one neutral polymer A and one weakly

<sup>a</sup> NIZO food research, Kernhemseweg 2, 6718 ZB Ede, The Netherlands

<sup>b</sup> Van 't Hoff Laboratory for Physical and Colloid Chemistry,  
Department of Chemistry, Debye Institute for Nanomaterials Science,  
Utrecht University, Padualaan 8, 3584 CH Utrecht, The Netherlands

<sup>c</sup> Laboratory of Physical Chemistry, Department of Chemical Engineering and  
Chemistry, Institute for Complex Molecular Systems, Eindhoven University of  
Technology, PO Box 513, 5600 MB Eindhoven, The Netherlands.  
E-mail: m.vis@tue.nl

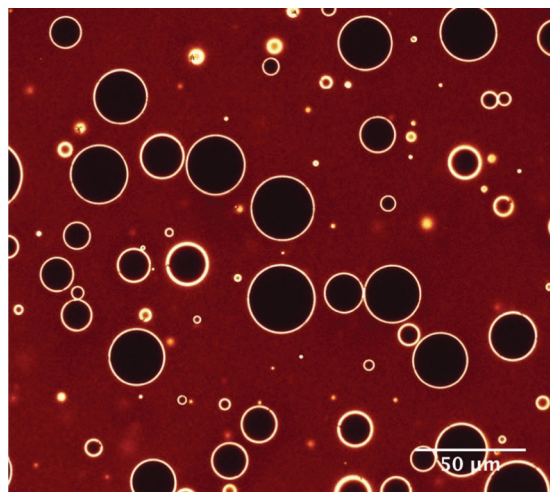


Fig. 1 Confocal micrograph of a mixture of dextran, gelatin and fluorescent FITC-dextran (imaged as red/yellow) at approximately neutral pH and  $\sim 10$  mM salt. The dextran is uncharged, the gelatin is weakly positively charged, and the FITC-dextran is weakly negatively charged. The droplets are dextran-rich, the continuous phase is gelatin-rich. The FITC-dextran accumulates primarily at the water–water interface of the droplets.

charged polymer B. Provided polymer B is only weakly charged and the salt concentration is high enough,<sup>10</sup> such a system still shows segregative phase separation into a phase rich in polymer A (phase  $\alpha$ ) and a phase rich in polymer B (phase  $\beta$ ). As an example, Fig. 2a shows phase diagrams from SCF computations on model systems. Fig. 2b shows the interfacial tension between the aqueous coexisting phases of these systems. Both phase behaviour and interfacial tension resemble trends seen in experimental systems.<sup>10–12,14,19,22–24</sup>

To arrive at interfacial complexation, we add a small amount of polyelectrolyte (PE), which is chemically similar to polymer A and has a charge opposite to polymer B. We presume that the PE is therefore attracted to phase  $\beta$  because of its charge, while at the same time it is also attracted to phase  $\alpha$  due to its chemistry. We hypothesize that, under appropriate conditions, the polyelectrolyte may therefore adsorb at the interface due to localized complexation.

While our study primarily focuses on self-consistent field theory, we qualitatively corroborate our findings with experimental results. Our experimental system consists of aqueous mixtures of dextran and (non-gelling) gelatin, a well-studied model system for studying water–water phase separation.<sup>11,12,19,25–27</sup> Dextran (polymer A) is uncharged, gelatin (polymer B) is weakly charged ( $pI \sim 9$ ). The polyelectrolyte is exemplified by dextran which has been chemically labelled with a small number of FITC groups, which have a carboxylic acid group with  $pK_a \sim 6.4$ . Because of the values for the  $pI$  of gelatin and the  $pK_a$  of FITC, there exists a pH window in which the FITC-dextran is oppositely charged to the gelatin, while maintaining chemical similarity to the dextran. Additionally, interfacial accumulation can easily be detected using confocal microscopy as FITC is fluorescent.

It is expected that interfacial complexation, or any accumulation of added polymer at an interface, may cause interfacial gelation,

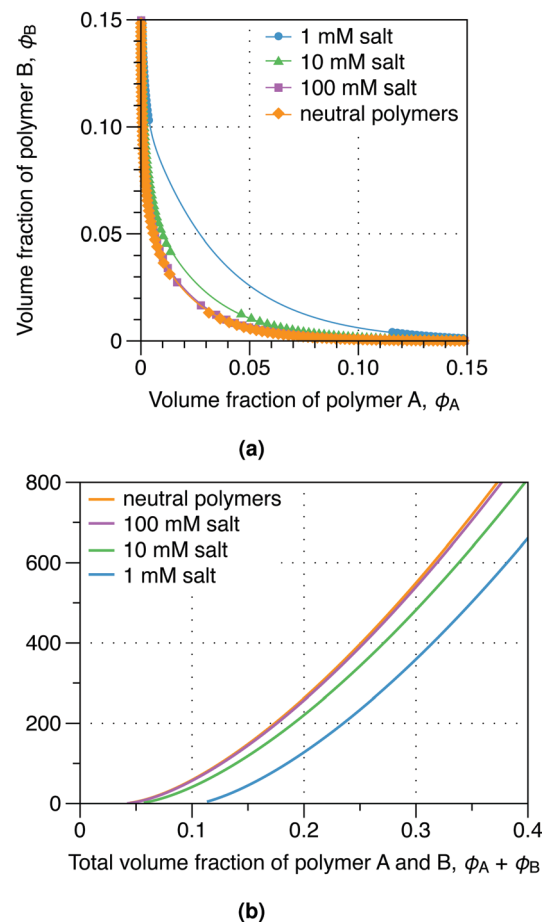


Fig. 2 (a) Phase diagram and (b) interfacial tension from self-consistent field computations on an aqueous mixture of neutral polymer A and charged polymer B ( $z_B = +3$ ) for various salt concentrations. Polymers A and B both have a degree of polymerisation  $N = 1000$ . The polymers are in a theta solvent ( $\chi_{AS} = \chi_{BS} = 0.5$ ) and are slightly mutually repulsive ( $\chi_{AB} = 0.05$ ), leading to phase separation. At high salt concentrations, the phase behaviour and interfacial tension are practically the same as for the case of two neutral polymers with the same interaction parameters.

changes in interfacial stiffness, and electrostatic or steric repulsions between water-in-water emulsion droplets. While water-in-water Pickering emulsions are well established,<sup>17,28–32</sup> interfacial complexation would provide a new route towards stabilizing fully water-based emulsions. Being able to stabilize water-in-water emulsions and in general control the properties of water–water interfaces will be of practical importance in several fields of applied science, such as encapsulation, flavour retention, replacement of ubiquitous oil-based emulsions in food systems,<sup>33</sup> and controlling bacterial growth in water-based mixtures. Studying water–water interfaces also fits well in the general trend to replace non-aqueous solvents by water.

The remainder of this article will be structured as follows. First, the experimental methods will be described, followed by a discussion of the theoretical methods. Next, the theoretical results will be described, discussed and qualitatively compared to experiments. The paper ends with general conclusions and an outlook.

## 2 Experimental methods

Cold-water fish gelatin (gelation temperature approximately 8 °C, molar mass 100 kDa) from Norland Products was kindly provided by FIB Foods B.V. (Harderwijk, The Netherlands). Dextran (molar mass 200 kDa) was purchased from Sigma-Aldrich. Both polymers were rather polydisperse, with  $M_w/M_n \sim 2.5$ . These polymers were used without purification. FITC-labeled dextran (molar mass 200 kDa) was prepared as described by de Belder & Granath.<sup>34</sup>

The degree of labelling was determined by spectroscopy at 500 nm and found to be  $0.009 \pm 0.001$  FITC labels per monomer of dextran, *i.e.*, on the order of 10 labels per chain. Dextran solutions (10% by mass) were prepared at room temperature by stirring for one to two hours. Gelatin solutions (10% by mass) were prepared by stirring at room temperature during one hour and after that stirring for one hour at 60 °C. FITC-labeled dextran was added at 0.1% to the 10% dextran solution.

Phase separating mixtures for observation by confocal microscopy were prepared as follows. Approximately 0.3 g of a 1% FITC-dextran solution was added to 10 g of a 10% dextran solution. 0.1 g of this solution was added to 10 g of 10% gelatin solution, resulting in a final mass fraction of FITC-dextran of  $3 \times 10^{-4}$  in the phase separating systems. Based on previous knowledge of the phase diagram of such systems,<sup>10</sup> we estimate that the coexisting phases had an approximately symmetrical composition and consisted for  $\sim 20\%$  by mass of one polymer and for a comparatively negligible amount ( $\sim 1\%$ ) of the other polymer. The salt concentration was of the order of  $\sim 10$  mM, due to residual salt present mainly in the gelatin. Experiments at increased salt concentration were performed in presence of 100 mM NaCl. Experiments at increased pH were conducted through addition of dilute NaOH. Confocal microscopy was carried out on a LEICA TCS SP Confocal Scanning Light microscope.

## 3 Theoretical methods

### 3.1 Self-consistent field theory

The self-consistent field (SCF) theory that is applied here to compute the thermodynamic properties of a solution containing charged and uncharged polymers is briefly outlined. The numerical lattice approximation of Scheutjens and Fleer<sup>35–37</sup> is used here.

In the Scheutjens–Fleer (SF-SCF) method, space is represented by a set of lattice sites and the molecules are represented by segments in such a way that one segment fits a given lattice site. For a given problem one needs to define a particular lattice geometry which allows a three-dimensional system be modelled using concentration gradients in either one, two, or three directions. It is obvious that computational efficiency rapidly decreases with increasing number of concentration gradients. For the present situation, one concentration gradient suffices, because the concentration is only expected to be a function of the distance to the interface.

For the application of SCF theory in this work, where the interest lies in liquid–liquid phase separation and the resulting

interface between the coexisting phases, the focus is on a flat geometry. Space is defined by the lattice layers numbered  $x = 0, 1, 2, \dots, T, T + 1$ . The system is bound by mirrors at lattice layers  $x = 0$  and  $x = T + 1$ . The total number of lattice layers  $T$  is chosen to be large to such a degree that the bulk concentrations of all components are attained.

In SCF theory, the Helmholtz free energy  $F$  is a function of the volume fraction  $\phi(x)$  and the corresponding local potential  $u(x)$ :<sup>37,38</sup>

$$F[\{\phi\}, \{u\}, \alpha] = -\ln Q(\{u\}) - \sum_x \sum_j u_j(x) \phi_j(x) + F^{\text{int}}(\{\phi\}) + \sum_x \alpha(x) \left( \sum_j \phi_j(x) - 1 \right). \quad (1)$$

It is noted that here and below all energies are normalized by the thermal energy  $k_B T$ . The subscript  $j$  refers to the type of unit filling a lattice site, which will be denoted as a segment and may be, *e.g.*, a monomer or solvent molecule. Here the system consists of the following segment types: neutral solvent molecules (S), positively and negatively charged ions, neutral polymer segments (A), weakly positively charged polymer segments (B) and negatively charged polyelectrolyte segments (PE). The polymer chains are modelled as linear polymers; each segment is treated with the restriction that it is covalently linked to 1 or 2 other segments. All segments are treated such that they occupy a single lattice site of size  $b$ .

We will now discuss all terms of eqn (1) consecutively. The first term is the partition function  $Q(\{u\}, V, T)$  for the ‘potential’ ensemble, which can be computed when the potentials are known. For the implementation of this term, a polymer chain model needs to be specified and explicit information on the chain architectures is required. The partition function  $Q$  of the system can be decomposed into single chain partition functions  $q_i$  for each type of molecule  $i$ , which may consist of one or more segments,

$$Q = \prod_i \frac{(q_i)^{n_i}}{n_i!}, \quad (2)$$

where  $n_i$  is the number of molecules (chains) of type  $i$ .

The single molecule partition function contains the combined statistical weights of all possible chain conformations. The freely-jointed chain model is used here to evaluate this quantity. In this model, chain reversals to previously occupied lattice sites are allowed, implying that self-avoiding chains are not accounted for. The rationale for choosing this chain model is that a very efficient propagator formalism exists for the freely-jointed chain model to obtain the single chain partition function, which is easily adapted for molecules with side chains. Basically,  $q_i$  contains the statistical weights of all possible and (in the freely jointed chain model) allowed conformations of molecule  $i$ .

Let, as an example, molecule  $i$  be composed of a linear chain with  $N_i$  segments labelled  $s = 1, \dots, N_i$ . Let  $\delta_{is}^j$  be unity when segment  $s$  of molecule  $i$  is of segment type  $j$ , and zero otherwise.

Then one can obtain the potential energy  $u_i^c$  of a given conformation  $c$  (a specified spatial arrangement of the segments of the chain) by summing over the potential energies of the segments along the chain of chain type  $i$ :

$$u_i^c = \sum_s \sum_j \delta_{is}^j u_j(r_{is}^c), \quad (3)$$

where  $r_{is}^c$  is the coordinate of segment  $s$  in conformation  $c$ . Now the partition function is given as

$$q_i = \sum_c \exp(-u_i^c). \quad (4)$$

In this form the computational effort to evaluate the partition function is enormous as it is proportional to the number of different conformations. Within the freely-jointed chain approximation, the neighbouring segments along the chain occupy neighbouring lattice sites and positional correlations of segments further apart are basically ignored. For a lattice coordination number  $Z$  (the number of nearest neighbour sites), there are  $Z^{N_i-1}$  number of conformations for a given starting position of the chain.

As mentioned already, there exists a propagator formalism which generates  $q_i$ . An important advantage of SF-SCF is that the propagator formalism allows the evaluation of the partition function with a computational effort proportional to  $N_i$ , which makes it typically  $10^4$  times faster than computer simulations. This scheme also automatically generates the volume fraction distribution  $\phi_i(r,s)$ . Summing these over all segments it is straightforward to generate the segment type dependent volume fractions  $\phi_j(r)$ . As a result we see that the volume fractions can be computed from knowledge of the segment potentials, more formally,  $\phi[u]$ .

The second term in eqn (1) is a Legendre transformation to turn the result into the NVT ensemble.<sup>37</sup> The third term in eqn (1) is the contribution that specifies all possible interactions including the electrostatic interactions between the different segments. Electrostatic interactions are accounted for by a lattice version of the Poisson equation. This amounts to a term proportional to

$$\sum_x \frac{1}{2} q(x) \psi(x) \quad (5)$$

in  $F^{\text{int}}$ , where  $q(x)$  is the sum of the charges at coordinate layer  $x$  and  $\psi(x)$  is the electrostatic potential. Here

$$q(x) = \sum_j \phi_j(x) e z_j^{\text{mon}} \quad (6)$$

with  $z_j^{\text{mon}}$  the valence or number of charges of a segment/monomer  $j$  and  $e$  the elementary charge. The electrostatic potential is found by solving the Poisson equation in flat geometry, which requires knowledge of the local dielectric permittivity  $\varepsilon(x)$ . This is computed as the volume fraction weighted average, that is

$$\varepsilon(x) = \varepsilon_0 \sum_j \phi_j(x) \varepsilon_{r,j}$$

with  $\varepsilon_0$  the permittivity of vacuum and  $\varepsilon_{r,j}$  the relative permittivity of a material composed fully of segments of type  $j$ .

The solvency effects are approximated in  $F^{\text{int}}$  by short-range nearest-neighbour interactions using the Bragg-Williams mean-field approximation.<sup>39</sup> Each contact between unlike segments (computed based on the local volume fractions) is characterized by a dimensionless Flory-Huggins interaction parameter  $\chi_{jk}$ , for contacts between segments of type  $j$  and  $k$ , which is positive for repulsive interactions and negative in case of attraction.<sup>39</sup> These parameters implement the usual convention that the like contacts  $jj$  and  $kk$  are taken as reference, see ref. 40.

The last term of eqn (1) imposes the incompressibility constraint

$$\sum_j \phi_j(x) = 1,$$

implemented locally at each position  $x$ . This term contains the Lagrange parameter  $\alpha(x)$ .

Optimization of the free energy provides the constraint

$$\frac{\partial F}{\partial \phi_j(x)} = 0, \quad (7)$$

yielding more specifically

$$u_j(x) = \alpha(x) + \frac{\partial F^{\text{int}}}{\partial \phi_j(x)}, \quad (8)$$

which enables to compute the self-consistent solutions of eqn (1). The local potential  $u_j(x)$  is the result of a combined contribution of the Lagrange field  $\alpha(x)$  and the derivative of the interaction. For details see ref. 41.

Because of the mean-field approximation, all interactions within a layer are smeared out. Although a general expression for  $u_j(x)$  is rather involved, in case of a binary solution (one polymer in a solvent) the potential energy  $u_j(x)$  of a certain segment in layer  $x$  relative to bulk is, as an example, given by<sup>42</sup>

$$u_j(x) = \chi[\langle 1 - 2\phi_j(x) \rangle - 1 + 2\phi_j^b] - \ln[1 - \phi_j(x)] + \ln[1 - \phi_j^b], \quad (9)$$

where the superscript  $b$  refers to the bulk concentration of segment  $j$ , taken as the volume fraction at the first or last lattice layer for large  $T$ . The angular brackets  $\langle \rangle$  denote a weighted average over three layers, which accounts for the fraction of contacts that a component  $j$  has with its nearest neighbours in these layers. For example, the average volume fraction of nearest-neighbour components of a site in layer  $x$  is given by

$$\langle \phi_j(x) \rangle = \lambda_1 \phi_j(x-1) + \lambda_0 \phi_j(x) + \lambda_1 \phi_j(x+1), \quad (10)$$

where  $\lambda_0$  is the fraction of lattice sites in contact with other sites in the same layer  $x$ . Similarly, a fraction  $\lambda_1$  is in contact with sites in a lower layer and another fraction  $\lambda_1$  with sites in a higher layer. In this study  $\lambda_0 = 2/3$  and  $\lambda_1 = 1/6$ .

The grand potential can be obtained from the SCF computations by subtracting the chemical potentials  $\mu_i$  of all molecules  $i$  from the Helmholtz free energy,

$$\Omega = F - \sum_i \mu_i n_i. \quad (11)$$



The evaluated grand potential directly provides the interfacial tension  $\gamma$  between the phases<sup>43</sup> in terms of  $\gamma b^2/k_B T$ , with  $b$  the lattice size.

### 3.2 Parameters

The model system that we consider in our SCF computations consists of two polymers A and B with a degree of polymerization  $N_A = N_B = 1000$ . We assume both polymers are in a theta solvent S, thus the  $\chi$ -parameters are  $\chi_{AS} = \chi_{BS} = 0.5$ . The polymers are slightly mutually repulsive,  $\chi_{AB} = 0.05$ , leading to phase separation. All calculations are for  $\phi_A = \phi_B$ , where  $\phi_i$  is the global volume fraction (*i.e.*, the average over the volume fraction profiles  $\phi_i(x)$ ). For two uncharged polymers, the critical demixing concentration is located at a global total polymer volume fraction  $\phi_A + \phi_B = 0.044$ , see Fig. 2.

In the remainder of our calculations, polymer A is uncharged while polymer B has a number of charges  $z_B = +3$ . The polyelectrolyte has the same degree of polymerization and  $\chi$  parameters as polymer A, to simulate its chemical similarity. It has a varying number of charges, from  $z_{PE} = 0$  to  $-100$ . The charge of polymer  $i$  is incorporated by giving all segment types  $j$  of which it is composed an equal fractional number of charges  $z_j^{\text{mon}} = z_i/N_i$ . In order to screen the charges, the system contains monovalent salt at concentrations of 1, 10 and 100 mM. The lattice size  $b = 0.3$  nm in all calculations and the system under consideration consists of  $T = 100$  lattice layers.

All calculations pertaining to the interfacial adsorption of polyelectrolyte were carried out at global volume fraction of polymers A and B of  $\phi_A = \phi_B = 0.2$ . In this way, the system is at a relatively large distance to the critical point regardless of salt concentration so that the volume fraction profiles  $\phi_i(x)$  of polymers A and B are nearly independent of salt concentration and the presence of a small amount of polyelectrolyte, which simplifies comparisons. Experimentally, such high volume fractions would be rather difficult to achieve as it would lead to extremely viscous solutions. We therefore only aim to model the experimental system in a qualitative way.

All SCF calculations are performed with the SFBBox software package.<sup>38</sup>

### 3.3 Analysis

For the present study, the main outcomes of our SCF calculations are the compositions of the coexisting phases (Fig. 2a), the volume fractions profiles  $\phi_i(x)$  of each component and the interfacial tension  $\gamma$  (Fig. 2b) of the system. We will quantify our results by calculating the following parameters.

**3.3.1 Distribution of polyelectrolyte over bulk phases.** The bulk distribution coefficient  $K_{\text{bulk}}$  of the polyelectrolyte is defined as

$$K_{\text{bulk}} \equiv \frac{\phi_{\text{PE}}^\alpha}{\phi_{\text{PE}}^\alpha + \phi_{\text{PE}}^\beta}, \quad (12)$$

where  $\phi_{\text{PE}}^\alpha$  and  $\phi_{\text{PE}}^\beta$  refer to the volume fractions of the polyelectrolyte in the bulk of phase  $\alpha$  and  $\beta$ , respectively. This parameter is calculated for the limit of low polyelectrolyte volume fractions, where the global PE volume fraction is  $\phi_{\text{PE}} = 10^{-7}$ . In words,  $K_{\text{bulk}}$  is unity if all polyelectrolyte resides in phase  $\alpha$  and

zero if all polyelectrolyte resides in phase  $\beta$ . A value of  $1/2$  indicates an equal distribution over the two phases.

### 3.3.2 Relative concentration of polyelectrolyte at interface.

The relative interfacial concentration  $K_{\text{int}}$  of the polyelectrolyte is defined as

$$K_{\text{int}} = \frac{\max \phi_{\text{PE}}(x)}{\max(\phi_{\text{PE}}^\alpha, \phi_{\text{PE}}^\beta)}. \quad (13)$$

The parameter  $K_{\text{int}}$  is the maximum volume fraction of the profile divided by the maximum of the two bulk volume fractions. By definition,  $K_{\text{int}} \geq 1$ . Like  $K_{\text{bulk}}$ , this parameter is also calculated for  $\phi_{\text{PE}} = 10^{-7}$ .

**3.3.3 Interfacial excess of polyelectrolyte.** The total amount of polyelectrolyte adsorbed at the water–water interface, or the interfacial excess, can be calculated by integrating the difference in volume fraction between bulk and interface. For component  $i$ , the excess is formally defined as

$$\theta_i = \int_{-\infty}^{x_{\text{Gibbs}}} dx [\phi_i(x) - \phi_i^\beta] + \int_{x_{\text{Gibbs}}}^{+\infty} dx [\phi_i(x) - \phi_i^\alpha], \quad (14)$$

where the distance  $x$  is (still) normalized by the lattice size. In our case, the first integral starts at the first lattice layer and the second integral runs up to the last lattice layer. We define the position  $x_{\text{Gibbs}}$  of the Gibbs dividing plane such that the excess of polymers A and B is equal,  $\theta_A = \theta_B$ . To account for the possibility that the Gibbs dividing plane may not lie exactly in the middle of two lattice layers, linear interpolation between lattice layers is used. The interfacial excess is calculated for various global PE volume fractions  $\phi_{\text{PE}}$ . The interpretation of  $\theta_i$  is that it is the volume fraction that would be obtained if all interfacial excess were accumulated into a single lattice layer. It relates to the adsorption density  $\Gamma_i$  (number of chains per unit area) as

$$\Gamma_i = \theta_i/(N_i b^2). \quad (15)$$

We will now describe and discuss our results using eqn (12) to (14) to quantitatively assess the adsorption of polyelectrolyte at a water–water interface.

## 4 Results and discussion

First the phase diagram and interfacial tension of the system is discussed. The phase diagrams computed using SCF in Fig. 2a show that, for aqueous mixtures of a neutral and weakly charged polymer, the phase behaviour depends strongly on the salt concentration. At lower salt concentrations, the binodal shifts to higher polymer concentrations, whereas at high salt concentrations the binodal is virtually indistinguishable from the case of two uncharged polymers in solution. This is also evidenced by Fig. 2b, where the start of macroscopic phase separation ( $\gamma > 0$ ) is shifted to higher volume fractions for lower salt concentrations. These effects are mainly due to ion entropy, as shown by earlier experimental and theoretical work.<sup>10,22–24</sup>

To investigate the behaviour of added polyelectrolyte, we first turn our attention to the interfacial volume fraction profiles shown in Fig. 3. The volume fraction profiles of polymer A and B

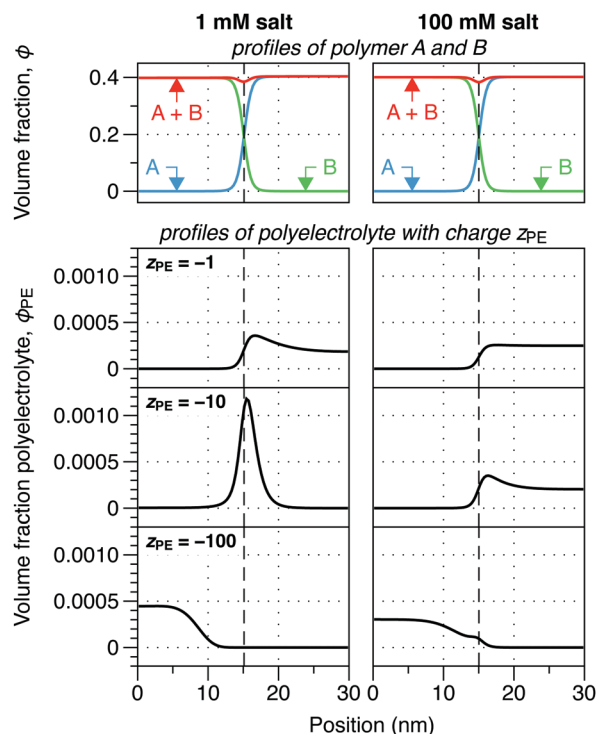


Fig. 3 (top) Interfacial volume fraction profiles of an aqueous mixture of neutral polymer A and charged polymer B ( $z_B = +3$ ) from self-consistent field computations. (bottom) Profiles of added polyelectrolyte PE ( $\phi_{PE} = 10^{-4}$ ). PE is chemically identical to A, except PE has a number of charges  $z_{PE}$  as indicated. The dashed lines indicate the position of the Gibbs dividing surface leading to equal interfacial excess of A and B.

(top panel) show that the interface is several nanometers wide. This interface is depleted of both polymers and enriched in solvent, which leads to fewer unfavourable contacts between A and B and reduces the interfacial tension.<sup>16,44</sup> Because  $\phi_A = \phi_B = 0.2$ , the distance to the critical point is quite large and there is very little difference between the profiles of A and B at 1 and 100 mM salt.

When polyelectrolyte is added ( $\phi_{PE} = 10^{-4}$ ), its density profile depends on salt concentration and PE charge, see Fig. 3 (bottom panel). In general, at low charge, the PE resides primarily in phase  $\alpha$ , due to its similarity with polymer A, while at high charge it accumulates mostly in phase  $\beta$ . At high salt concentrations, the effects appear less pronounced than at low salt concentrations. However, for both high and low salt concentrations there appears to be an intermediate charge regime where the polyelectrolyte accumulates at the interface.

The distribution of polyelectrolyte in profiles such as those in Fig. 3 can be quantified using the bulk distribution coefficient  $K_{bulk}$  and the relative interfacial concentration  $K_{int}$ , eqn (12) and (13). Fig. 4 shows these as a function of the polyelectrolyte charge  $z_{PE}$  for 1, 10 and 100 mM salt. For all salt concentrations, there are regimes where the PE resides almost completely in one of the bulk phases. In between those regimes, where  $K_{bulk} \approx 0.5$ , the water–water interface is significantly enriched in polyelectrolyte: the concentration at the interface is locally  $10^2$  to  $10^3$  times higher than in bulk.

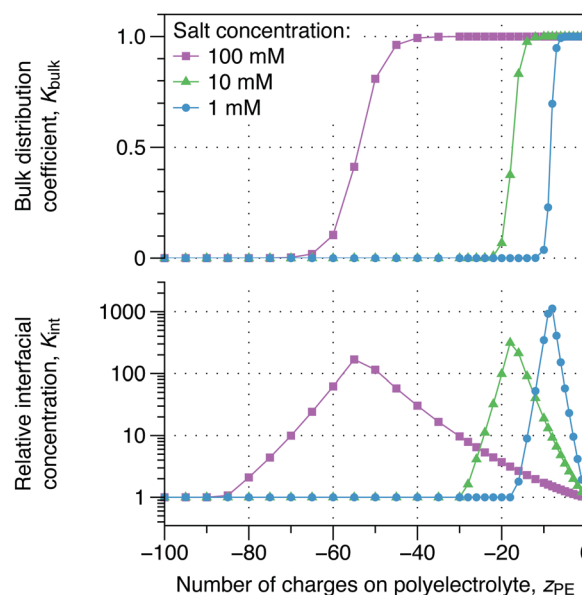


Fig. 4 (top) Bulk distribution coefficient  $K_{bulk}$  and (bottom) relative interfacial concentration  $K_{int}$  (eqn (12) and (13)) of polyelectrolyte PE as a function of its charge  $z_{PE}$  for various salt concentrations from self-consistent field computations. Besides PE, the system consists of neutral polymer A and charged polymer B ( $\phi_A = \phi_B = 0.2$ ,  $z_B = +3$ ). PE is chemically identical to A, except for its charge.  $K_{bulk} = 1$  means that all PE is in phase  $\alpha$  (polymer A-rich);  $K_{bulk} = 0$  means that all PE is in phase  $\beta$  (polymer B-rich). The data have been extracted from profiles such as depicted in Fig. 3.

A way to quantify the total amount of adsorbed polyelectrolyte is using the interfacial excess  $\theta_{PE}$ , eqn (14), shown in Fig. 5a as a function of  $\phi_{PE}$ . The values of the polyelectrolyte charge  $z_{PE}$  correspond to the maxima of  $K_{int}$  (Fig. 4, bottom panel); as a reference  $z_{PE} = 0$  is also shown, which displays no adsorption regardless of salt concentration.

At 1 mM salt, there is positive adsorption for  $z_{PE} = -8$ . For  $z_{PE} = -18$  and  $-55$ , there is negative adsorption: the polyelectrolyte resides fully in the bulk of phase  $\beta$ . This behaviour can also be seen in Fig. 3 for  $z_{PE} = -100$ . When increasing the salt concentration to 10 mM, there is positive adsorption for  $z_{PE} = -8$  and  $-18$ . At low polyelectrolyte volume fractions,  $z_{PE} = -18$  displays the most adsorption, but at higher volume fractions the adsorption remains constant while the interfacial excess continues to grow for  $z_{PE} = -8$ . Finally, at 100 mM salt, there is positive adsorption for  $z_{PE} = -8$ ,  $-18$  and  $-55$ . At low volume fractions,  $z_{PE} = -55$  features the most adsorption, which levels off at higher volume fractions.

The dashed line in Fig. 5a indicates the interfacial excess  $\theta_{PE}$  that would be obtained if all added polyelectrolyte would adsorb at the interface. At low volume fractions, the PE is indeed almost fully situated at the interface in some cases, which correspond to the maxima in  $K_{int}$  of Fig. 4. At higher volume fractions, adsorption levels off and polyelectrolytes with fewer charges sometimes adsorb to a greater extent. This hints that the interfacial accumulation stops because too much negative charge accumulates at the interface, making further adsorption unfavourable.

It is also interesting to note that the addition of a large amount of salt does not necessarily deplete the interface of all

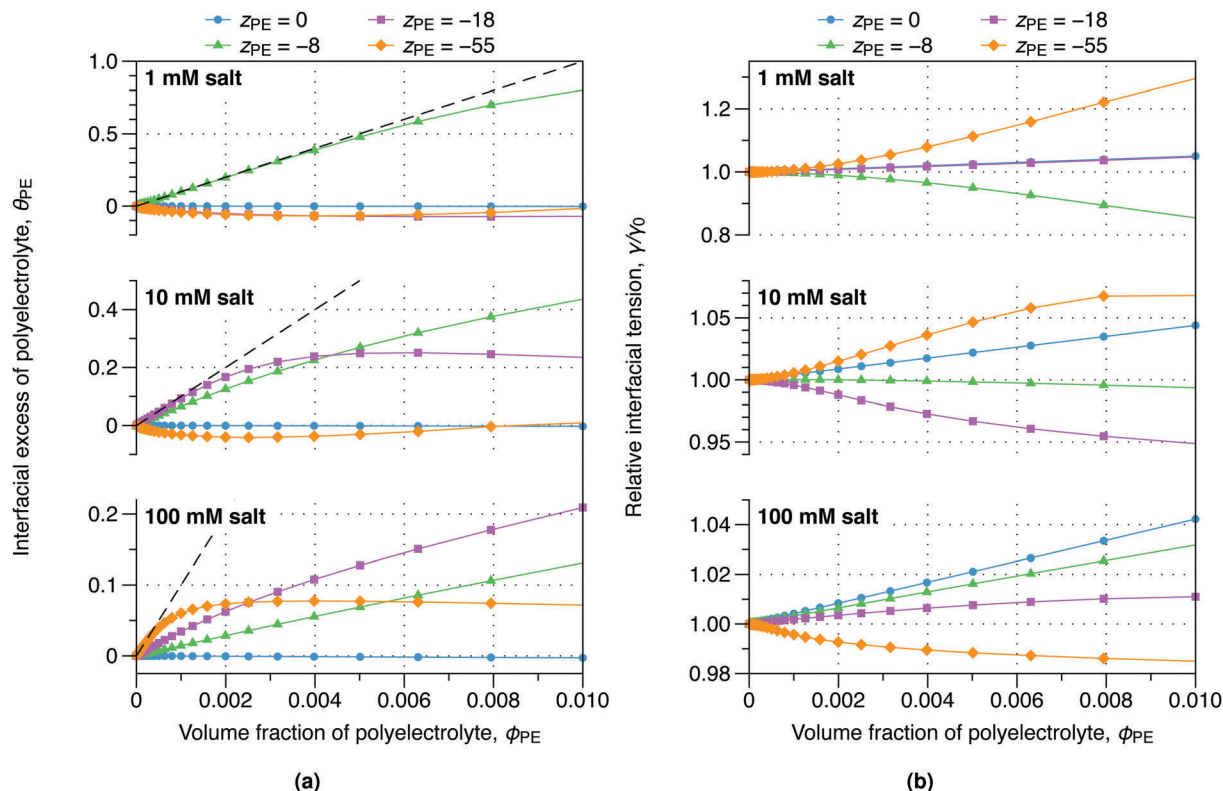


Fig. 5 (a) Interfacial excess  $\theta_{PE}$  of a polyelectrolyte PE and (b) relative interfacial tension  $\gamma/\gamma_0$  for an aqueous mixture of neutral polymer A and charged polymer B ( $z_B = +3$ ) from self-consistent field computations. Both are shown as a function of PE volume fraction for various polyelectrolyte charges  $z_{PE}$  and salt concentrations. The charges correspond to the maxima of  $K_{int}$  in Fig. 4. As a reference, the case  $z_{PE} = 0$  is also shown. For (a), the dashed line indicates  $\theta_{PE}$  if all PE were adsorbed.

polyelectrolyte excess. For instance, for  $z_{PE} = -8$ , going from 1 to 100 mM salt does indeed reduce the interfacial excess  $\theta_{PE}$ , but only by a factor  $\sim 7$ ; significant adsorption remains.

The effect of additional polyelectrolyte on the interfacial tension  $\gamma$  also deserves attention and is shown in Fig. 5b, relative to the tension  $\gamma_0$  without polyelectrolyte. Generally, positive adsorption

corresponds to a decrease of the interfacial tension. For weakly or non-adsorbing cases (*e.g.*  $z_{PE} = 0$ ), there is a minute increase in  $\gamma$ . Since the PE is chemically similar to polymer A, the addition of PE effectively increases the volume fraction of polymer A. This results in an increase in the distance to the critical point and therefore in the interfacial tension.

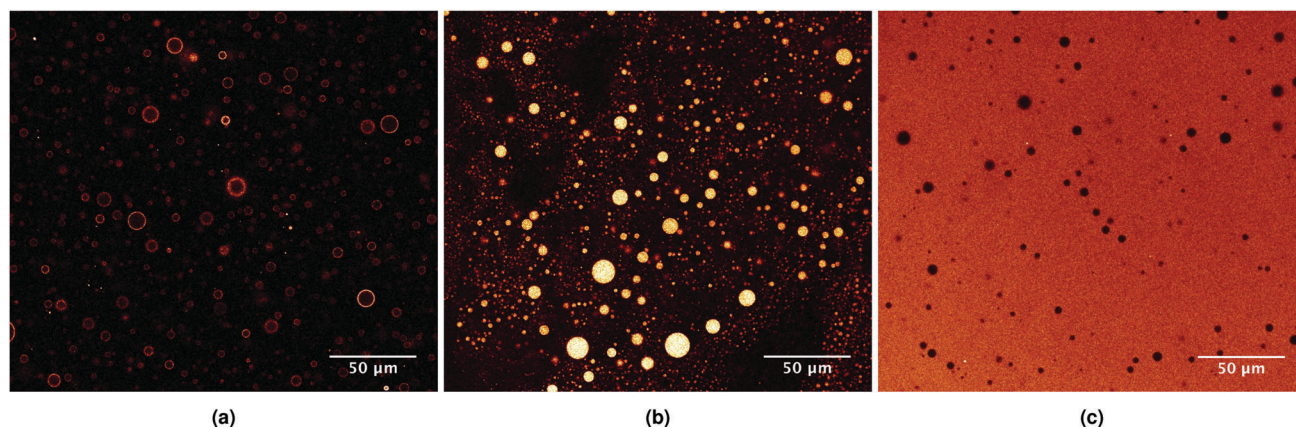


Fig. 6 Confocal micrographs of aqueous mixtures of dextran and gelatin under various conditions. The droplets are the dextran-rich phase, the continuous phase is gelatin-rich. Dextran is uncharged, gelatin has a pH-dependent charge. (a) At approximately neutral pH with 100 mM salt, gelatin is weakly positively charged. Added negatively charged fluorescent FITC-dextran (imaged as red/yellow) accumulates (weakly) at the interface. (b) At pH  $\approx 11$  with  $\sim 10$  mM salt, gelatin is weakly negatively charged. Negatively charged FITC-dextran resides in the dextran-rich droplets. (c) At approximately neutral pH with  $\sim 10$  mM salt, gelatin is weakly positively charged. Added FITC (not bound to dextran) accumulates fully in the gelatin-rich continuous phase.



The effects on the interfacial tension are rather small and do not correspond to that typical of surfactants at oil–water interfaces. The reason is that, while the total amount of adsorbed material  $\theta_{\text{PE}}$  may be large, it is the adsorption density  $\Gamma_{\text{PE}}$  (number of chains per unit area, eqn (15)) that drives the decrease of interfacial tension according to the Gibbs adsorption equation,

$$-d\gamma = \sum_i \Gamma_i d\mu_i. \quad (16)$$

As  $\Gamma_i$  is small for polymers due to their high molar mass, the change in  $\gamma$  is also small. We therefore postulate that, if polyelectrolytes in practice turn out to stabilize water-in-water emulsions, it is not as a consequence of a decrease in the interfacial tension (as would be the case for, e.g., microemulsions), but because they provide a barrier against coalescence, through for instance interfacial gelation, steric stabilization, or electrostatic repulsions.

Finally, we compare the outcomes of our calculations with experimental observations. Fig. 6a shows an aqueous mixture of neutral dextran (polymer A), weakly positively charged gelatin (polymer B) and weakly negatively charged FITC-dextran (PE) with 100 mM salt. Despite the high salt concentration, there is still interfacial accumulation of the charged, fluorescent polymer, as predicted by theory (cf. Fig. 1, which shows the same system with only  $\sim 10$  mM salt). In the experiments, interfacial accumulation is only suppressed at high pH, where the gelatin (polymer B) is negatively charged, just as the FITC-dextran. In that case, all negatively charged FITC-dextran migrates to the dextran-rich droplets, see Fig. 6b. Under the circumstances where FITC-dextran adsorbs at the interface, plain FITC (not bound to dextran) instead resides in the gelatin-rich phase, see Fig. 6c. This corroborates the idea that the interfacial accumulation of dextran-FITC is driven by the competition of affinity for both phases.

## 5 Conclusions

We theoretically studied the behaviour of polyelectrolytes at water–water interfaces in a model system consisting of neutral polymer A and weakly positively charged polymer B in a common solvent. When the polyelectrolyte is chemically similar to polymer A, but oppositely charged to polymer B, strong accumulation of the polyelectrolyte at the water–water interface is observed, as shown by our self-consistent field computations. This adsorption is driven by two competitive interactions. On one hand, the polyelectrolyte prefers contact with polymer A over contact with B due to chemical composition; on the other hand, there are electrostatic attractions between polyelectrolyte and polymer B. We hypothesize the resulting adsorption to be complexation localized at the water–water interface. Although the adsorption is strong, the effect on interfacial tension is small. Adsorption of polyelectrolytes may cause interfacial gelation, changes in interfacial stiffness, and steric or electrostatic repulsions of droplets in water-in-water emulsions. This complexation is predicted to persist even at high salt concentration, which is relevant from the perspective of (food) applications. The complexation of

polyelectrolytes at water–water interfaces offers the perspective of a new route towards stable fully aqueous emulsions, which is of practical importance for many applications such as in food science and pharmacy.

## Acknowledgements

The authors would like to thank F. A. M. Leermakers for useful discussions and providing the SFBox software package. M. V. would like to thank D. Erp for stimulating discussions.

## References

- 1 H. G. Bungenberg de Jong and H. R. Kruyt, *Proc. K. Ned. Akad. Wet.*, 1929, **32**, 849–856.
- 2 L. De Ruiter and H. G. Bungenberg de Jong, *Proc. K. Ned. Akad. Wet.*, 1947, **50**, 836–848.
- 3 I. Michaeli, J. T. G. Overbeek and M. J. Voorn, *J. Polym. Sci.*, 1957, **23**, 443–450.
- 4 J. T. G. Overbeek and M. J. Voorn, *J. Cell. Comp. Physiol.*, 1957, **49**, 7–26.
- 5 F. Weinbreck, R. H. Tromp and C. G. de Kruif, *Biomacromolecules*, 2004, **5**, 1437–1445.
- 6 M. Antonov, M. Mazzawi and P. L. Dubin, *Biomacromolecules*, 2010, **11**, 51–59.
- 7 E. Spruijt, J. Sprakel, M. A. Cohen Stuart and J. van der Gucht, *Soft Matter*, 2010, **6**, 172–178.
- 8 M. W. Beijerinck, *Zentralbl. Bakteriöl., Parasitenkd. Infektionsskrankh.*, 1896, **22**, 697–699.
- 9 V. Y. Grinberg and V. B. Tolstoguzov, *Food Hydrocolloids*, 1997, **11**, 145–158.
- 10 M. Vis, V. F. D. Peters, B. H. Ern  and R. H. Tromp, *Macromolecules*, 2015, **48**, 2819–2828.
- 11 E. Scholten, R. Tuinier, R. H. Tromp and H. N. W. Lekkerkerker, *Langmuir*, 2002, **18**, 2234–2238.
- 12 P. Ding, B. Wolf, W. J. Frith, A. H. Clark, I. T. Norton and A. W. Pacek, *J. Colloid Interface Sci.*, 2002, **253**, 367–376.
- 13 M. Vis, B. H. Ern  and R. H. Tromp, *Biointerphases*, 2016, **11**, 018904.
- 14 V. G. Langhammer and L. Nestler, *Makromol. Chem.*, 1965, **88**, 179–187.
- 15 E. Scholten, L. M. C. Sagis and E. van der Linden, *Biomacromolecules*, 2006, **7**, 2224–2229.
- 16 D. Broseta, L. Leibler, L. O. Kaddour and C. Strazielle, *J. Chem. Phys.*, 1987, **87**, 7248.
- 17 M. Vis, J. Opdam, I. S. J. van't Oor, G. Soligno, R. van Roij, R. H. Tromp and B. H. Ern , *ACS Macro Lett.*, 2015, **4**, 965–968.
- 18 M. Vis, V. F. D. Peters, R. H. Tromp and B. H. Ern , *Langmuir*, 2014, **30**, 5755–5762.
- 19 M. Vis, V. F. D. Peters, E. M. Blokhuis, H. N. W. Lekkerkerker, B. H. Ern  and R. H. Tromp, *Phys. Rev. Lett.*, 2015, **115**, 078303.
- 20 Q. Ma, Y. Song, J. W. Kim, H. S. Choi and H. C. Shum, *ACS Macro Lett.*, 2016, **5**, 666–670.
- 21 S. D. Hann, T. H. R. Niepa, K. J. Stebe and D. Lee, *ACS Appl. Mater. Interfaces*, 2016, **8**, 25603–25611.



- 22 M. B. Perrau, I. Iliopoulos and R. Audebert, *Polymer*, 1989, **30**, 2112–2117.
- 23 K. Bergfeldt and L. Piculell, *J. Phys. Chem.*, 1996, **100**, 5935–5940.
- 24 V. B. Tolstoguzov, *Food Hydrocolloids*, 1991, **4**, 429–468.
- 25 M. W. Edelman, E. van der Linden, E. H. A. de Hoog and R. H. Tromp, *Biomacromolecules*, 2001, **2**, 1148–1154.
- 26 V. Y. Grinberg, V. B. Tolstoguzov and G. L. Slonimskii, *Vysokomol. Soedin., Ser. A*, 1970, **12**, 1593–1599.
- 27 P. Van Puyvelde, Y. A. Antonov and P. Moldenaers, *Food Hydrocolloids*, 2002, **16**, 395–402.
- 28 A. T. Poortinga, *Langmuir*, 2008, **24**, 1644–1647.
- 29 H. Firoozmand, B. S. Murray and E. Dickinson, *Langmuir*, 2009, **25**, 1300–1305.
- 30 G. Balakrishnan, T. Nicolai, L. Benyahia and D. Durand, *Langmuir*, 2012, **28**, 5921–5926.
- 31 T. Nicolai and B. Murray, *Food Hydrocolloids*, DOI: 10.1016/j.foodhyd.2016.08.036.
- 32 J. Esquena, *Curr. Opin. Colloid Interface Sci.*, 2016, **25**, 109–119.
- 33 H. McGee, *McGee on food & cooking: an encyclopedia of kitchen science, history and culture*, Hodder & Stoughton, 2004.
- 34 A. De Belder and K. Granath, *Carbohydr. Res.*, 1973, **30**, 375–378.
- 35 J. M. H. M. Scheutjens and G. J. Fleer, *J. Phys. Chem.*, 1979, **83**, 1619–1635.
- 36 G. J. Fleer, M. A. Cohen Stuart, J. M. H. M. Scheutjens, T. Cosgrove and B. Vincent, *Polymers at interfaces*, Chapman and Hall, London, 1993.
- 37 F. A. M. Leermakers, J. C. Eriksson and J. Lyklema, *Fundamentals of Interface and Colloid Science*, Elsevier, Amsterdam, 2005, vol. 5.
- 38 J. van Male, PhD thesis, Wageningen University, 2003.
- 39 P. J. Flory, *Principles of Polymer Chemistry*, Cornell University Press, Ithaca, NY, 1953.
- 40 O. A. Evers, J. M. H. M. Scheutjens and G. J. Fleer, *Macromolecules*, 1990, **23**, 5221–5233.
- 41 Y. Lauw, F. A. M. Leermakers and M. A. Cohen Stuart, *J. Phys. Chem. B*, 2003, **107**, 10912–10918.
- 42 G. J. Fleer, *Adv. Colloid Interface Sci.*, 2010, **159**, 99–116.
- 43 R. Tuinier and G. J. P. Krooshof, *J. Colloid Interface Sci.*, 2012, **382**, 105–109.
- 44 R. H. Tromp and E. M. Blokhuis, *Macromolecules*, 2013, **46**, 3639–3647.